Discontinuous Galerkin Time-Domain Method for GPR Simulation in Dispersive Media

Tiao Lu, Wei Cai, and Pingwen Zhang

***Abstract*—This paper presents a newly developed high-order discontinuous Galerkin time-domain (DGTD) method for solving Maxwell's equations in linear dispersive media with UPML boundary treatment. A unified formulation is derived for linear dispersive media of Debye type and the artificial material in the UPML regions with the help of auxiliary differential equations. The DGTD employs finite-element-type meshes, and uses piecewise high-order polynomials for spatial discretization and Runge–Kutta method for time integrations. Arbitrary high-order accuracy can be obtained for scattering of various objects in dispersive media. After validating the numerical convergence of the DGTD method together with the second-order Yee's scheme, we apply this new method to the ground-penetrating radar for the detection of buried objects in a lossy half space.**

***Index Terms*—Discontinuous Galerkin time-domain (DGTD), dispersive media, ground-penetrating radar (GPR), perfectly matched layer (PML).**

I. Introduction

TIME-DOMAIN methods of electromagnetic scattering can provide important transient and broadband frequency information of scattering waves. There have been recent efforts in developing high-order time-domain methods beyond the traditional second-order Yee's scheme [1] for the application of ground-penetrating radar (GPR) in dispersive media [2], [3]. In order to achieve higher order results, it is critical to avoid accuracy degeneracy of the numerical methods due to the material interfaces of the inhomogeneous media. Several remedies have been proposed to avoid the accuracy degeneracy of Yee's scheme and the Cartesian grid-based method by modifying the difference formulas near the material interfaces, and second-order results have been obtained [4], [5]. On the other hand, discontinuous Galerkin time-domain (DGTD) methods have been shown to have the flexibility of handling material interfaces with high-order accuracy by using finite-element triangulation of the inhomogeneous media [6]–[11]. The DGTD shares some similarity with the multidomain pseudospectral time-domain method of [3] in using high-order polynomials over a finite-element type of mesh. However, the unique feature of DGTD is the fact that the numerical solutions are allowed to be discontinuous across element interfaces where numerical fluxes are defined in a manner to guarantee the conservation of physical quantities. As the solutions are allowed to be discontinuous, DGTD provides the capability to approximate discontinuous fields accurately across the material interfaces in inhomogeneous media in addition to the high-order accuracy where the media and fields are continuous.

For scattering in dispersive media, such as GPR in the earth soil, the numerical methods should also be able to handle efficiently the frequency dependence of the dielectric constant and the constitutive relations to the same degree of accuracy of the discretization of the Maxwell equations. For time-domain simulation methods, the frequency dependence of the dielectric constant implies a temporal convolution of the the susceptibility and the electric field, resulting in expensive storages of the history of the electric fields. Several types of techniques have been proposed to avoid this storage, including recursive convolution (RC) and piecewise linear recursive convolution (PLRC) [12]–[14], auxiliary differential equations (ADEs) [15]–[17], and Z-transform (ZT) [18]. As we are using a high-order discontinuous Galerkin method, the ADE method has been shown [11] to handle this convolution in time to the same order of accuracy as the spatial discretization of the DGTD. The frequency dependence of the material property could also come from the introduction of the PML layers [19]–[21] used to terminate the computational domain. In [11], we have introduced a unified DGTD formulation to solve transverse magnetic (TM) Maxwell's equations in the linear Debye dispersive media and in the uniaxial PML (UPML) region. The UPML [20], [21] is incorporated with the DGTD allowing us to treat the frequency dependence of the dielectric constant of the soil dispersive media and the artificial dispersive media of the UPML region in a unified way. Highly accurate results have been obtained for scattering in dispersive media [11]. In this paper, we will apply this newly developed DGTD to the GPR in dispersive earth media.

In Section II, we will present the unified formulation with ADE methods for both TM and transverse electric (TE) waves for electric dispersive media of the Debye type. Section III will cover the discontinuous Galerkin time-domain method based on the formulation of Section II. In Section IV, we present several numerical validations of the proposed DGTD in comparison with Yee's finite-difference scheme, and then, applications to GPR in dispersive soil media. Finally, a conclusion is given in Section V.

II. Formulation

In [11], we have presented a unified formulation of DGTD for the TM Maxwell equations in the dispersive media and the

Manuscript received February 11, 2004; revised July 30, 2004. The work of W. Cai was supported in part by the U.S. National Science Foundation under Grants CCR-0098275 and DMS-0408309. The work of P. Zhang was supported in part by the National Science Foundation of China under Grant 90207009 and in part by Distinguished Young Scholars Grant 10225103.

T. Lu and P. Zhang are with the Laboratory of Mathematics and Mechanization (LMAM) and the School of Mathematical Sciences, Peking University, Beijing 100871, China (e-mail: pzhang@pku.edu.cn).

W. Cai is with the Department of Mathematics, University of North Carolina, Charlotte, NC 28223 USA (e-mail: wcai@uncc.edu).

Digital Object Identifier 10.1109/TGRS.2004.838350

UPML regions where ADE methods are used to handle the temporal convolution of the electric field. Here, we will give the unified formulation for both TM and TE Maxwell equations for completeness for electric dispersive media of the Debye type.

A. TE and TM Waves: Maxwell's Equations in Debye Dispersive Materials and PML Regions

Consider an inhomogeneous, conductive, and electrically dispersive medium with relative magnetic permeability u_r and conductivity σ. Here, we consider a single-pole Debye medium with the electric susceptibility in frequency domain expressed as

$$\chi(\omega) = \frac{\epsilon_{r,s} - \epsilon_{r,\infty}}{1 + j\omega\tau} = \frac{\Delta\epsilon_r}{1 + j\omega\tau}$$

where $\epsilon_{r,s}$ is the static zero-frequency relative electric permittivity, $\epsilon_{r,\infty}$ is the infinite-frequency relative electric permittivity, $\Delta\epsilon_r$ is the change in relative permittivity, and τ is the pole relation time. The Maxwell's equations for TM and TE cases in dispersive media and UPML regions are given as follows. The equations are reduced to the normal Maxwell equations in the physical media when the UPML parameters $\sigma_x = 0, \sigma_y = 0$.

TM case:

$$\begin{aligned}
\epsilon_\infty \frac{\partial E_z}{\partial t} &= \frac{\partial H_y}{\partial x} - \frac{\partial H_x}{\partial y} - c_0 E_z - P_{z,1} \\
&\quad - c_1 P_{z,2} - \sigma\sigma_x\sigma_y P_{z,3} \\
\mu \frac{\partial H_x}{\partial t} &= -\frac{\partial E_z}{\partial y} - \mu\frac{\sigma_y - \sigma_x}{\epsilon_0} H_x + Q_x \\
\mu \frac{\partial H_y}{\partial t} &= \frac{\partial E_z}{\partial x} - \mu\frac{\sigma_x - \sigma_y}{\epsilon_0} H_y + Q_y \\
\tau \frac{\partial P_{z,1}}{\partial t} &= -P_{z,1} + c_2 E_z + c_3 P_{z,2} \\
\epsilon_0 \frac{\partial P_{z,2}}{\partial t} &= E_z \\
\epsilon_0 \frac{\partial P_{z,3}}{\partial t} &= P_{z,2} \\
\epsilon_0 \frac{\partial Q_x}{\partial t} &= -\sigma_x Q_x + \frac{\mu\sigma_x(\sigma_y - \sigma_x)}{\epsilon_0} H_x \\
\epsilon_0 \frac{\partial Q_y}{\partial t} &= -\sigma_y Q_y + \frac{\mu\sigma_y(\sigma_x - \sigma_y)}{\epsilon_0} H_y.
\end{aligned} \tag{1}$$

TE case:

$$\begin{aligned}
\mu \frac{\partial H_z}{\partial t} &= -\frac{\partial E_y}{\partial x} + \frac{\partial E_x}{\partial y} - \frac{\mu(\sigma_x + \sigma_y)}{\epsilon_0} H_z - \mu Q_z \\
\epsilon_\infty \frac{\partial E_x}{\partial t} &= \frac{\partial H_z}{\partial y} - c_0 E_x + \frac{\Delta\epsilon}{\tau} P_{x,1} - c_4 P_{x,2} \\
\epsilon_\infty \frac{\partial E_y}{\partial t} &= -\frac{\partial H_z}{\partial x} - c_0 E_y + \frac{\Delta\epsilon}{\tau} P_{y,1} - c_4 P_{y,2} \\
\epsilon_0^2 \frac{\partial Q_z}{\partial t} &= \sigma_x\sigma_y H_z \\
\tau \frac{\partial P_{x,1}}{\partial t} &= -P_{x,1} + E_x + P_{x,2} \\
\epsilon_0 \frac{\partial P_{x,2}}{\partial t} &= -\sigma_x P_{x,2} + (\sigma_y - \sigma_x) E_x \\
\tau \frac{\partial P_{y,1}}{\partial t} &= -P_{y,1} + E_y + P_{y,2} \\
\epsilon_0 \frac{\partial P_{y,2}}{\partial t} &= -\sigma_y P_{y,2} + (\sigma_x - \sigma_y) E_y
\end{aligned} \tag{2}$$

where

$$\begin{aligned}
&\epsilon_\infty = \epsilon_0\epsilon_{r,\infty} \quad \Delta\epsilon = \epsilon_0\Delta\epsilon_r \quad \mu = \mu_0\mu_r \\
&c_0 = \Delta\epsilon/\tau + \sigma + \epsilon_{r,\infty}(\sigma_x + \sigma_y) \\
&c_1 = \sigma_x\sigma_y + \sigma(\sigma_x + \sigma_y) \\
&c_2 = -\Delta\epsilon/\tau + \Delta\epsilon_r(\sigma_x + \sigma_y) \\
&c_3 = \Delta\epsilon_r\sigma_x\sigma_y \\
&c_4 = \Delta\epsilon/\tau + \sigma - \epsilon_{r,\infty}
\end{aligned}$$

and P and Q are the auxiliary polarization variables.

B. DGTD Method

The spatial discretization of the DGTD is based on a Galerkin approximation procedure for the spatial derivatives,, while the time integration is done using high-order Runge–Kutta methods. First, the computational domain will be decomposed into elements K (triangles or quadrilaterals); then, on each element K, the field components and the auxiliary variables are expressed in terms of polynomial basis functions. The numerical solutions $\mathbf{U}$ are allowed to be discontinuous across interfaces between the elements; however, a unique numerical flux $\mathbf{h}_K(\mathbf{U}^-, \mathbf{U}^+)$ will be defined along the interface using the solution values on both sides of the interface, i.e., $\mathbf{U}^-, \mathbf{U}^+$. We will illustrate the procedure for the case of the TM wave. Equation (1) can be written in a vector form as

$$\frac{\partial \mathbf{U}^{(1)}}{\partial t} + \nabla \cdot \left(\mathbb{A}\mathbf{U}^{(1)}\right) = \mathbf{S}^{(1)} \tag{3}$$

$$\frac{\partial \mathbf{U}^{(2)}}{\partial t} = \mathbf{S}^{(2)} \tag{4}$$

where

$$\begin{aligned}
\mathbf{U}^{(1)} &= (\epsilon_\infty E_z, \mu H_x, \mu H_y)^T \\
\mathbf{U}^{(2)} &= (P_{z,1}, P_{z,2}, P_{z,3}, Q_x, Q_y)^T \\
\mathbb{A} &= (A_x, A_y)
\end{aligned}$$

and

$$A_x = \begin{pmatrix} 0 & 0 & -1/\mu \\ 0 & 0 & 0 \\ -1/\epsilon_\infty & 0 & 0 \end{pmatrix}$$

$$A_y = \begin{pmatrix} 0 & 1/\mu & 0 \\ 1/\epsilon_\infty & 0 & 0 \\ 0 & 0 & 0 \end{pmatrix}$$

$$\mathbf{S}^{(1)} = \begin{pmatrix} -c_0 E_z - P_{z,1} - c_1 P_{z,2} - \sigma\sigma_x\sigma_y P_{z,3} \\ -\mu(\sigma_y - \sigma_x) H_x/\epsilon_0 + Q_x \\ -\mu(\sigma_x - \sigma_y) H_y/\epsilon_0 + Q_y \end{pmatrix} \tag{5}$$

$$\mathbf{S}^{(2)} = \begin{pmatrix} (-P_{z,1} + c_2 E_z + c_3 P_{z,2})/\tau \\ E_z/\epsilon_0 \\ P_{z,2}/\epsilon_0 \\ -\sigma_x Q_x/\epsilon_0 + \mu\sigma_x(\sigma_y - \sigma_x) H_x/\epsilon_0^2 \\ -\sigma_y Q_y/\epsilon_0 + \mu\sigma_y(\sigma_x - \sigma_y) H_y/\epsilon_0^2 \end{pmatrix}. \tag{6}$$

Basis function space $\mathcal{P}(K)$: Let $\mathcal{T}_h$ be a triangulation of the solution domain Ω, and ϵ_∞ and μ are assumed constant on each element $K \in \mathcal{T}_h$. We denote a finite-dimensional space of smooth functions defined on an element K by $\mathcal{P}(K)$. This

space will be used to approximate solution $\mathbf{U} = (\mathbf{U}^{(1)}, \mathbf{U}^{2)})^T$. Setting

$$V_h := \{v \in L^1(\Omega) \,|\, v|_K \in \mathcal{P}(K) \qquad \forall K \in \mathcal{T}_h\}. \quad (7)$$

To define the basis function space $\mathcal{P}(K)$ on an element K, we first construct a set of basis functions on a standard reference element I; then, using the mapping $\mathbf{\Psi}$, we can obtain a set of basis functions on the physical element K. For example, we can define a set of basis functions on the standard reference triangle element I

$$P_n^2 = \text{span}\{\xi^i \eta^j; 0 \le i+j \le n\} = \text{span}\{\phi_j(\xi,\eta)\}_{j=1}^N$$

where n is the maximum order of the polynomial and $N = (n+2)(n+1)/2$. For triangular elements, if higher order basis $(n > 7)$ is desired, Dubiner orthogonal polynomial basis functions [22] have been shown to provide well-conditioned mass matrices (25) and yield exponential convergence for even discontinuous fields [23].

A set of basis functions for the standard rectangle element I can be chosen as

$$\text{span}\{L_i(\xi)L_j(\eta); 0 \le i+j \le n\} = \text{span}\{\phi_j(\xi,\eta)\}_{j=1}^N$$

where $L_i(\cdot)$ is the Legendre polynomial of order i and $N = (n+2)(n+1)/2$.

And the set of basis functions on each physical element K is obtained by the mapping $\mathbf{\Psi}$ as

$$\text{span}\{\phi_j(\xi(x,y),\eta(x,y)); 1 \le j \le N\}$$

where $(\xi,\eta) = \mathbf{\Psi}^{-1}(x,y)$.

Next the electric field E_z and magnetic field H_x and H_y are represented in terms of the basis functions $\phi_j(\boldsymbol{x}), \boldsymbol{x} = (x,y) \in K$

$$E_{z,N}(\boldsymbol{x},t) = \sum_{j=1}^N E_{z,j}\phi_j(\boldsymbol{x}) \quad (8)$$

$$H_{w,N}(\boldsymbol{x},t) = \sum_{j=1}^N H_{w,j}\phi_j(\boldsymbol{x}), \qquad w = x,y. \quad (9)$$

Here, $E_{z,j}$ and $H_{x,j}, H_{y,j}$ are the time-dependent coefficients. And $\mathbf{U}^{(2)}$ is also approximated by the basis functions

$$P_{z,s,N}(\boldsymbol{x},t) = \sum_{j=1}^N P_{z,s,j}\phi_j(\boldsymbol{x}), \qquad s = 1,2,3 \quad (10)$$

$$Q_{w,N}(\boldsymbol{x},t) = \sum_{j=1}^N Q_{w,j}\phi_j(\boldsymbol{x}), \qquad w = x,y. \quad (11)$$

Galerkin approximation: To derive the spatial discretization for (3) and (4), we multiply both sides of the equations by a test function $v_h \in V_h$ and integrate over each element K, and we transfer the gradient operator in $\nabla\cdot(\mathbb{A}\mathbf{U}^{(1)})$ to the test function v_h using integration by parts. Then, the DGTD space discretization of the hyperbolic system for the eight-component vector $\mathbf{U}$ is formulated as follows. Find $\mathbf{U} \in V_h^8$ such that, for all $v_h \in V_h$ and on each element K

$$\int_K \left(\frac{\partial \mathbf{U}^{(1)}}{\partial t} v_h - \mathbf{S}^{(1)} v_h - \mathbb{A}\mathbf{U}^{(1)} \cdot \nabla v_h\right) d\boldsymbol{x} + \int_{\partial K} \mathbf{h}_K\left(\mathbf{U}^{(1),-}, \mathbf{U}^{(1),+}\right) \cdot \hat{\boldsymbol{n}}_K v_h ds = 0 \quad (12)$$

$$\int_K \left(\frac{\partial \mathbf{U}^{(2)}}{\partial t} v_h - \mathbf{S}^{(2)} v_h\right) d\boldsymbol{x} = 0 \quad (13)$$

where $\hat{\boldsymbol{n}}_K = (n_x, n_y)$ is the outward unit normal to ∂K, $\mathbf{U}^{(1),-}$ and $\mathbf{U}^{(1),+}$ are the values of the solution $\mathbf{U}$ on each side of the boundary ∂K of K, defined as

$$\mathbf{U}^{(1),\pm}(\boldsymbol{x}) = \lim_{\delta -> 0^+} \mathbf{U}^{(1)}(\boldsymbol{x} \pm \delta \hat{\boldsymbol{n}}_k)$$

and the numerical flux $\mathbf{h}_K(\mathbf{U}^{(1),-}, \mathbf{U}^{(1),+})$ is an approximation to $\hat{\boldsymbol{n}}_K \cdot \mathbb{A}\mathbf{U}^{(1)}|_{\partial K}$ on the faces of the element K, which satisfies the following consistent condition:

$$\mathbf{h}_K\left(\mathbf{U}^{(1)}, \mathbf{U}^{(1)}\right) = \hat{\boldsymbol{n}}_K \cdot \mathbb{A}\mathbf{U}^{(1)}\Big|_{\partial K}. \quad (14)$$

For the TM wave, we have shown in [11] that

$$\mathbf{h}_K\left(\mathbf{U}^{(1),-}, \mathbf{U}^{(1),+}\right) = \left(h_K^{E_z}, h_K^{H_x}, h_K^{H_y}\right)^T = \begin{pmatrix} -\frac{[Z(n_xH_y - n_yH_x) - E_z]^- + [Z(n_xH_y - n_yH_x) + E_z]^+}{Z^- + Z^+} \\ n_y \frac{[YE_z - (n_xH_y - n_yH_x)]^- + [YE_z + (n_xH_y - n_yH_x)]^+}{Y^- + Y^+} \\ -n_x \frac{[YE_z - (n_xH_y - n_yH_x)]^- + [YE_z + (n_xH_y - n_yH_x)]^+}{Y^- + Y^+} \end{pmatrix} \quad (15)$$

where $Z^\pm = (\epsilon_\infty^\pm/\mu^\pm)^{1/2}$ and $Y = 1/Z$ are the local impedance and admittance, respectively.

From the duality of the TE$_z$ and TM$_z$ cases, the numerical flux for the TE$_z$ case can be obtained by replacing E_z with H_z, replacing H_x by $-E_x$, and replacing H_y by $-E_y$, replacing Z by Y and replacing Y by Z in (15)

$$\mathbf{h}_K(\mathbf{U}^{(1),-}, \mathbf{U}^{(1),+}) = \left(h_K^{H_z}, h_K^{E_x}, h_K^{E_y}\right)^T = \begin{pmatrix} \frac{[Y(n_xE_y - n_yE_x) + H_z]^- + [Y(n_xE_y - n_yE_x) - H_z]^+}{Y^- + Y^+} \\ -n_y \frac{[ZH_z + (n_xE_y - n_yE_x)]^- + [ZH_z - (n_xE_y - n_yE_x)]^+}{Z^- + Z^+} \\ n_x \frac{[ZH_z + (n_xE_y - n_yE_x)]^- + [ZH_z - (n_xE_y - n_yE_x)]^+}{Z^- + Z^+} \end{pmatrix} \quad (16)$$

where $\mathbf{U}^{(1)} = (\mu H_z, \epsilon_\infty E_x, \epsilon_\infty E_y)^T$.

By setting $v_h = \phi_j(\boldsymbol{x}), 1 \le j \le N$ on each element K, a system of ODEs will be obtained for the expansion coefficients (8)–(11) of the field and auxiliary variables.

ODEs for unknowns: On each element K, we define the unknown vectors

$$\mathbf{E}^z = (E_{z,1}, E_{z,2}, \ldots, E_{z,N})^T$$
$$\mathbf{H}^x = (H_{x,1}, H_{x,2}, \ldots, H_{x,N})^T$$
$$\mathbf{H}^y = (H_{y,1}, H_{y,2}, \ldots, H_{y,N})^T$$
$$\mathbf{P}^{z,s} = (P_{z,s,1}, P_{z,s,2}, \ldots, P_{z,s,N})^T, \qquad s = 1,2,3$$
$$\mathbf{Q}^w = (Q_{w,1}, Q_{w,2}, \ldots, Q_{w,N})^T, \qquad w = x,y$$

and also the basis function vector

$$\boldsymbol{\phi} = (\phi_1, \phi_2, \ldots, \phi_N)^T.$$

Now, assuming that $\epsilon_{r,\infty}, \mu_r, \sigma_x, \sigma_y, \tau, \sigma$ are constant on each element, using the Gauss quadrature formulation to evaluated the integration in (12)–(13), we can obtain the following ODEs for the unknown vectors:

$$\frac{d\mathbf{E}^z}{dt} = -\frac{1}{\epsilon_\infty M}\left(M^x\mathbf{H}^y + M^y\mathbf{H}^x + M\mathbf{S}_N^{E_z} + \int_{\partial K} h_K^{E_z}\boldsymbol{\phi}\, ds\right) \quad (17)$$

$$\frac{d\mathbf{H}^x}{dt} = \frac{1}{\mu M}\left(M^y\mathbf{E}^z + M\mathbf{S}_N^{H_x} - \int_{\partial K} h_K^{H_x}\boldsymbol{\phi}\, ds\right) \quad (18)$$

$$\frac{d\mathbf{H}^y}{dt} = -\frac{1}{\mu M}\left(M^x\mathbf{E}^z + M\mathbf{S}_N^{H_y} - \int_{\partial K} h_K^{H_y}\boldsymbol{\phi}\, ds\right) \quad (19)$$

where

$$\begin{aligned}
\mathbf{S}_N^{E_z} &= \left(S_1^{E_z}, S_2^{E_z}, \ldots, S_N^{E_z}\right)^T \\
S_j^{E_z} &= -c_0E_{z,j} - P_{z,1,j} - c_1P_{z,2,j} - \sigma\sigma_x\sigma_yP_{z,3,j} \\
\mathbf{S}_N^{H_x} &= \left(S_1^{H_x}, S_2^{H_x}, \ldots, S_N^{H_x}\right)^T \\
S_j^{H_x} &= -\mu(\sigma_y - \sigma_x)H_{x,j} + Q_{x,j} \\
\mathbf{S}_N^{H_y} &= \left(S_1^{H_y}, S_2^{H_y}, \ldots, S_N^{H_y}\right)^T \\
S_j^{H_y} &= -\mu(\sigma_x - \sigma_y)H_{y,j} + Q_{y,j}.
\end{aligned}$$

And for the auxiliary variables, we have

$$\frac{dP_{z,1,j}}{dt} = \frac{1}{\tau}\left(-P_{z,1,j} + c_2E_{z,j} + c_3P_{z,2,j}\right) \quad (20)$$

$$\frac{dP_{z,2,j}}{dt} = \frac{1}{\epsilon_0}E_{z,j} \quad (21)$$

$$\frac{dP_{z,3,j}}{dt} = \frac{1}{\epsilon_0}P_{z,2,j} \quad (22)$$

$$\frac{dQ_{x,j}}{dt} = -\frac{\sigma_x}{\epsilon_0}Q_{x,j} + \frac{\mu_r\sigma_x(\sigma_y - \sigma_x)}{\epsilon_0^2}H_{x,j} \quad (23)$$

$$\frac{dQ_{y,j}}{dt} = -\frac{\sigma_y}{\epsilon_0}Q_{y,j} + \frac{\mu_r\sigma_y(\sigma_x - \sigma_y)}{\epsilon_0^2}H_{y,j}. \quad (24)$$

Here, we have introduced the local mass matrix

$$M_{ij} = \int_K \phi_i(\boldsymbol{x})\phi_j(\boldsymbol{x})d\boldsymbol{x} \quad (25)$$

and two local stiffness matrices

$$\begin{aligned}
M_{ij}^x &= \int_K \frac{\partial\phi_i(\boldsymbol{x})}{\partial x}\phi_j(\boldsymbol{x})d\boldsymbol{x} \\
M_{ij}^y &= \int_K \frac{\partial\phi_i(\boldsymbol{x})}{\partial y}\phi_j(\boldsymbol{x})d\boldsymbol{x}.
\end{aligned}$$

C. Time Integration

The ODE systems (17)–(24) can be recast in the matrix format

$$\frac{d\mathbf{W}}{dt} = L(t, \mathbf{W})$$

where

$$\mathbf{W} = (\mathbf{E}^z, \mathbf{H}^x, \mathbf{H}^y, \mathbf{P}^{z,1}, \mathbf{P}^{z,2}, \mathbf{P}^{z,3}, \mathbf{Q}^x, \mathbf{Q}^y)^T$$

and $L(t, \mathbf{W})$ stands for the right-side terms in (17)–(24).

The solution is integrated in time with s stage Runge–Kutta method

$$\mathbf{W}^{n+1} = \mathbf{W}^n + \Delta t\sum_{i=1}^{s}\omega_i\mathbf{K}_i \quad (26)$$

where

$$\begin{aligned}
&\mathbf{K}_1 = L(t^n, \mathbf{W}^n) \\
&\mathbf{K}_i = L\left(t^n + \alpha_i\Delta t, \mathbf{W}^n + \Delta t\sum_{j=1}^{i-1}\beta_{ij}\mathbf{K}_j\right), \qquad i = 2, \ldots, s
\end{aligned} \quad (27)$$

where ω_i, α_i, and β_{ij} are the parameters of Runge–Kutta methods [24]. We used a four-stage fourth-order method given in [24]. But for general Runge–Kutta methods, a fifth-order method would require six stages. However for linear problems, one can achieve sth-order Runge–Kutta methods with s stages for any s. There are some complications with explicit time t dependency, and one can refer to [25] and [26].

III. Numerical Results

In this section, we will first compare the DGTD with the traditional Yee finite-difference scheme for the scattering of a dispersive cylinder and study their convergence; then, we will apply the DGTD for the GPR detection of buried objects in soil media.

A. Numerical Convergence: Scattering Wave of a Dispersive Square Cylinder

To demonstrate the high-order accuracy of the DGTD for dispersive media, we consider the scattering of a dispersive square cylinder, which is embedded in a dielectric medium with the relative permittivity $\epsilon_r = 4$ and the relative permeability $\mu_r = 1$. The square cylinder is aligned with the grid mesh line so the Yee's scheme could retain its second-order accuracy. The dispersive square cylinder is of Debye medium having a Debye pole with parameters $\epsilon_{r,\infty} = 9, \epsilon_{r,s} = 16, \sigma = 0.0004$ S/m, $\tau = 6.4 \times 10^{-11}$ s. A TM_z wave is excited by a current line source and scattered by the dispersive square ($[-0.42, 0.42] \times [-0.42, 0.42]$) cylinder [Fig. 2(a)]. The source is an electric line current source in z direction J_z

$$J_z = E_0\delta(x - x_c, y - y_c)f(t) \quad (28)$$

where $E_0 = \epsilon_r \epsilon_0$, and (x_c, y_c) is the location of the source. Here, $f(t)$ is an Gaussian pulse

$$f(t) = \exp(-((t-t_0)/t_{\text{decay}})^2) \tag{29}$$

where $t_0 = 0.9/f_{\text{cent}}, t_{\text{decay}} = t_0/4$, and the center frequency $f_{\text{cent}} = 500$ MHz.

Yee's scheme: In Yee's FDTD algorithm, the δ-function is approximated as

$$\delta(x - x_c, y - y_c) \approx \frac{1}{\Delta x \Delta y}$$

where Δx and Δy are the increments of the FDTD grid along the x and y axes, respectively. The (x_c, y_c) is assumed to coincide with an FDTD node of the Yee grid (i_c, j_c). The increment of the grid $\Delta = \Delta x = \Delta y = 0.008$ m, the time step $\Delta t = \Delta/2v = 2/75$ ns, where $v = c/2$ is the velocity of the light in the background, and c is the velocity of the light in free space.

Using the notations of [27], the FDTD expressions in nondispersive domain are given as

$$E_z|_{i,j}^{n+1} = E_z|_{i,j}^{n} + \frac{\Delta t}{\epsilon \Delta} \begin{pmatrix} H_y|_{i+1/2,j}^{n+1/2} - H_y|_{i-1/2,j}^{n+1/2} \\ -H_x|_{i,j-1/2}^{n+1/2} + H_x|_{i,j-1/2}^{n+1/2} \end{pmatrix} - \frac{\Delta t}{\Delta} f((n+1/2)\Delta t)\delta_{i,i_c}\delta_{j,j_c} \tag{30}$$

$$H_x|_{i,j+1/2}^{n+1/2} = H_x|_{i,j+1/2}^{n-1/2} - \frac{\Delta t}{\mu \Delta}\left(E_z|_{i,j+1}^{n} - E_z|_{i,j}^{n}\right) \tag{31}$$

$$H_y|_{i+1/2,j}^{n+1/2} = H_y|_{i+1/2,j}^{n-1/2} + \frac{\Delta t}{\mu \Delta}\left(E_z|_{i+1,j}^{n} - E_z|_{i,j}^{n}\right). \tag{32}$$

Meanwhile, in the dispersive domain, the FDTD methods are

$$E_z|_{i,j}^{n+1} = C_a E_z|_{i,j}^{n} + C_b \begin{pmatrix} H_y|_{i+1/2,j}^{n+1/2} - H_y|_{i-1/2,j}^{n+1/2} \\ -H_x|_{i,j-1/2}^{n+1/2} + H_x|_{i,j-1/2}^{n+1/2} \end{pmatrix} + \frac{C_b}{\Delta} P_z|_{i,j}^{n+1/2} \tag{33}$$

where

$$C_a = \frac{1 - [\sigma + \Delta\epsilon/\tau]\Delta t/2\epsilon_\infty}{1 + [\sigma + \Delta\epsilon/\tau]\Delta t/2\epsilon_\infty}$$
$$C_b = \frac{\Delta t/\epsilon_\infty \Delta}{1 + [\sigma + \Delta\epsilon/\tau]\Delta t/2\epsilon_\infty}$$
$$P_z|_{i,j}^{n+3/2} = D_a P_z|_{i,j}^{n+1/2} + D_b E_z|_{i,j}^{n+1} \tag{34}$$

where

$$D_a = \frac{1 - \Delta t/2\tau}{1 + \Delta t/2\tau} \quad D_b = \frac{(\epsilon_{r,s} - \epsilon_{r,\infty})\Delta t/\tau^2}{1 + \Delta t/2\tau}.$$

The computational domain is terminated with a third-order Mur's absorbing boundary condition [27] (similar accuracy was obtained with UPML boundary conditions).

DGTD with UPML: For the DGTD, the computational domain is decomposed into rectangles and fourth-order basis functions and fourth-order Runge–Kutta method are used. The δ-function is approximated as

$$\delta(x - x_c, y - y_c) \approx \sum_{i=1}^{N} f_i \phi_i \tag{35}$$

where $\phi_i, i = 1, 2, \ldots, N$ are the basis functions and f_i satisfies

$$\int_{K_c} \sum_{i=1}^{N} f_i \phi_i \phi_j \, dx \, dy = \phi_j(x_c, y_c), \qquad 1 \le j \le N \tag{36}$$

where (x_c, y_c) is assumed to be at the center of the square element K_c. The initial computational domina is $[-1.02, 1.02] \times [-1.02, 1.02]$.

The UPML parameter $\sigma_x(x)$ is set to be polynomial profile [27]

$$\sigma_x(x) = (l/d)^m \sigma_{x,\max} \tag{37}$$

where l is the distance from the interface between the PML and the physical solution domain, and d is the thickness of the PML. The definition of $\sigma_y(y)$ is similar. Equation (37) increases the value of the PML's σ_x from zero at $l = 0$, the surface of the PML, to $\sigma_{x,\max}$ at $l = d$, the PEC outer boundary. The reflection factor is

$$R(\theta) = e^{-2\eta\sigma_{x,\max} d\epsilon_{r,\infty}\cos\theta/(m+1)} \tag{38}$$

where η is the PML's characteristic wave impedance, and θ is the incident angle. Let m, d, and the desired reflection error $R(0)$ be known; then $\sigma_{x,\max}$ can be computed as

$$\sigma_{x,\max} = -\frac{(m+1)\ln(R(0))}{2\eta d \epsilon_{r,\infty}}. \tag{39}$$

For the computation below, we have set $R(0) = e^{-16}, m = 3$. In order to demonstrate the accuracy of the DGTD, we select the width of the UPML such that the reflection error from the UPML is negligible compared with the discretization error of DGTD. First, we compute with the DGTD with a fine mesh $\Delta x = 0.01$ with a 20-cell PML of thickness 0.2 and use the result as a reference. To gauge the error from PML for mesh $\Delta x = 0.04$,, we compute with two different PML widths (10 and 15 cells) and then compare the results against the result obtained on the finer mesh $\Delta x = 0.01$. Fig. 1 shows that errors for $\Delta x = 0.04$ are of the same order for both the 10- and 15-cell UPML; thus, the error of the numerical results is mainly from the DGTD spatial and time discretization.

Convergence study in L^2-norm of the error: We define L^2-norm of the error of the two numerical results $E_z^{(1)}$ and $E_z^{(2)}$ as

$$\left\| E_z^{(1)} - E_z^{(2)} \right\|_2 = \sqrt{\int_0^T \left(E_z^{(1)}(t) - E_z^{(2)}(t)\right)^2 cdt} \tag{40}$$

where c is the velocity of the light in free space, and $E_z^{(w)}(t)$ ($w = 1$ or 2) is the linear interpolation function.

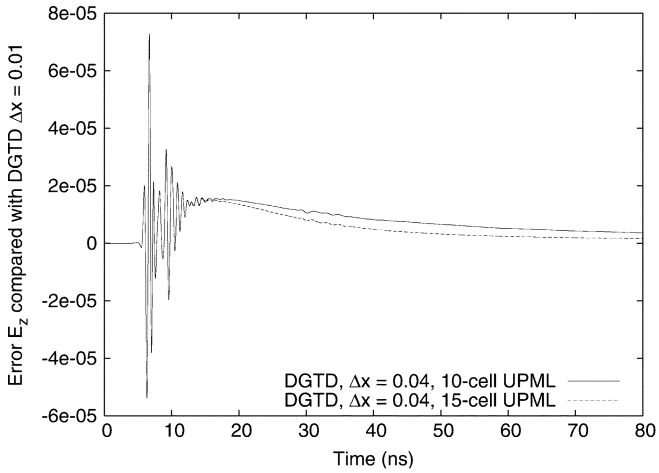

Fig. 1. Error of scattered wave E_z of two choices of UPML regions. One uses 10-cell UPML, and the other uses 15-cell UPML. The reference E_z is computed by the DGTD with grid size $\Delta x = 0.01$.

FDTD results over three meshes with grid sizes 0.008, 0.008/3, and 0.008/9 are denoted by $E^{F,1}, E_z^{F,2}$, and $E_z^{F,3}$, respectively, while DGTD results for three meshes with grid sizes 0.04, 0.02, and 0.01 by $E_z^{D,1}, E_z^{D,2}, E_z^{D,3}$, respectively. It has been found that $\|E^{F,1} - E_z^{F,2}\|_2 = 9.865 \times 10^{-3}, \|E^{F,2} - E_z^{F,3}\|_2 = 3.614 \times 10^{-3}$, $\|E^{F,1} - E_z^{F,3}\|_2 = 1.307 \times 10^{-2}$, and $\|E_z^{D,1} - E_z^{D,2}\|_2 = 5.022 \times 10^{-5}, \|E_z^{D,2} - E_z^{D,3}\|_2 = 8.730 \times 10^{-7}$, and $\|E_z^{D,1} - E_z^{D,3}\|_2 = 5.054 \times 10^{-5}$, which shows the convergence of both methods, as the mesh is refined with better convergence for the DGTD. The error convergence order of DGTD is 5.58, while the convergence rate for the FDTD is only 1.17, which shows the degeneracy of Yee's scheme near material interfaces. Also, by comparing the results of two methods, we found that $\|E_z^{F,1} - E_z^{D,3}\|_2 = 1.524 \times 10^{-2}, \|E_z^{F,2} - E_z^{D,3}\|_2 = 6.551 \times 10^{-3}$, and $\|E_z^{F,3} - E_z^{D,3}\|_2 = 3.959 \times 10^{-3}$ thus, both methods converge to the same solution.

Fig. 2(b) shows the numerical incident field E_z computed by FDTD and DGTD. Fig. 2(c) shows the calculated scattered field E_z.

We normalize the scattered field (E_z^s) spectrum by the incident field (E_z^i) spectrum and define the relative scattered power spectrum as

$$P(\omega) = 20 \log_{10} \left| \frac{E_z^s(\omega)}{E_z^i(\omega)} \right|.$$

Fig. 3 shows the relative scattered power spectral amplitudes.

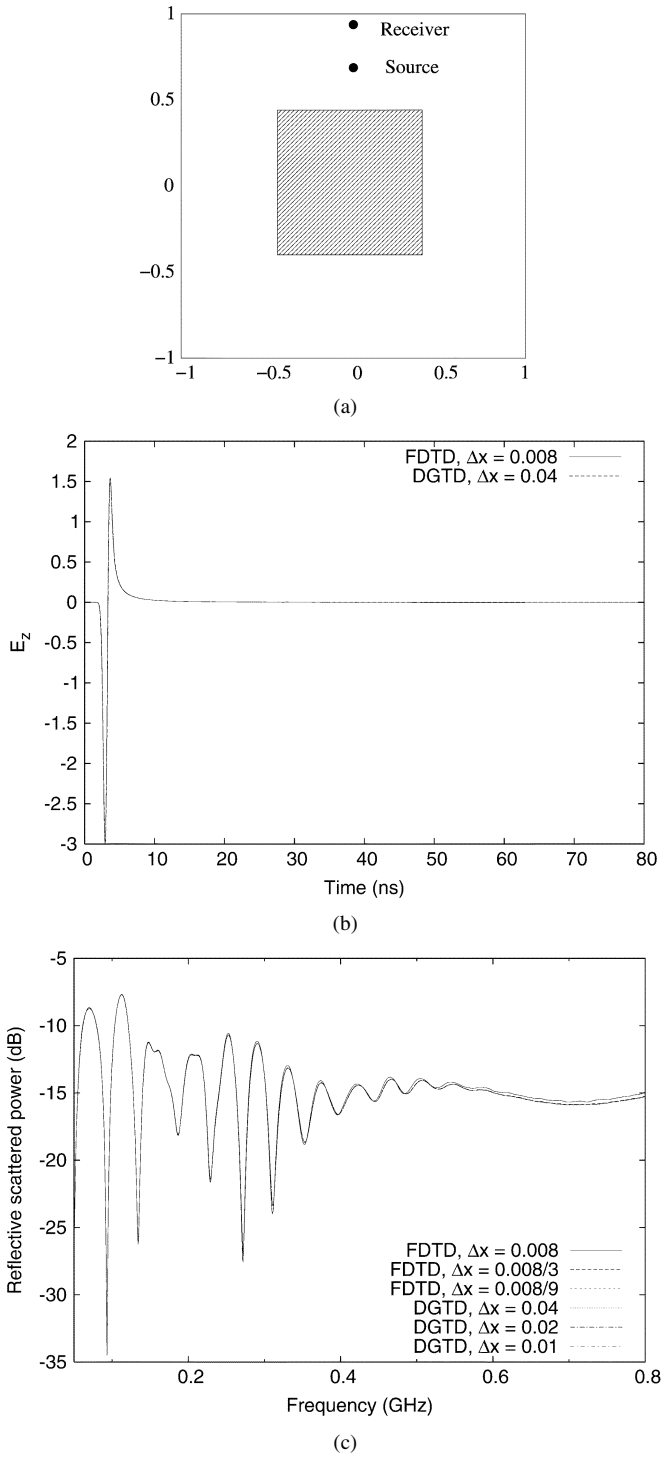

Fig. 2. (a) Dispersive nonrotated square cylinder. (b) The incident wave computed by two algorithms, FDTD and DGTD. (c) The scattering wave computed by two algorithms, FDTD and DGTD.

B. Scattering Wave of a Rotated Dispersive Square Cylinder

In this example, we will compute the scattering of a dispersive cylinder not aligned with the grid lines [the cylinder of Fig. 4(a)]. It is well known that Yee's scheme will have accuracy degeneracy due to the staircase problem [27]. However, the numerical results of the DGTD show its high-order accuracy as long as the mesh triangulation conforms to the geometry of the scatter. The source and receiver are located at (0, 0.7) and (0, 0.9), respectively. The line source and the parameters of the media are the same as the previous example.

Fig. 4(b) shows the numerical scattered field E_z. Three meshes with sizes $\Delta x = 0.04, \Delta x = 0.02$, and $\Delta x = 0.01$ are used, and their numerical scattered fields E_z are denoted by $E_z^{0.04}, E_z^{0.02}$, and $E_z^{0.01}$. The L^2-norms of the difference between them are $\|E_z^{0.04} - E_z^{0.02}\|_2 = 5.114 \times 10^{-5}$,

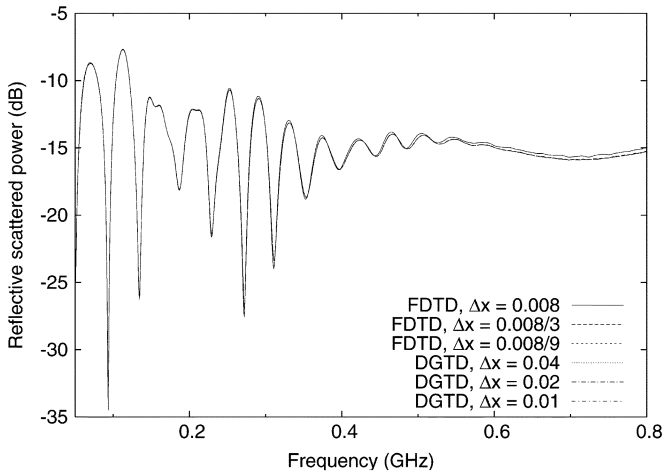

Fig. 3. Relative scattered power of spectral amplitude $P = 20\log_{10}|E_z^s(\omega)/E_z^i(\omega)|$ of a nonrotated square cylinder.

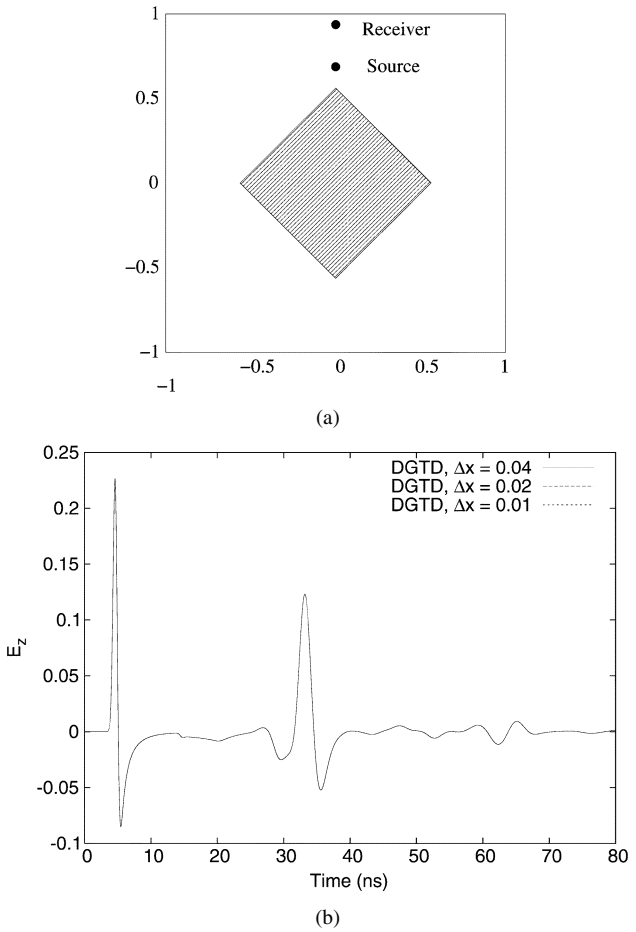

Fig. 4. (a) Dispersive nonrotated square cylinder. (b) The scattering wave computed by DGTD. Two DGTD meshes of sizes $\Delta x = 0.04, \Delta x = 0.02$, and $\Delta x = 0.01$ are used.

$\|E_z^{0.02} - E_z^{0.01}\|_1 = 8.448 \times 10^{-7}$, and $\|E_z^{0.04} - E_z^{0.01}\|_1 = 5.108 \times 10^{-5}$. The error convergence order is 5.92.

C. GPR Detection of Buried Objects

In this example, we will simulates the detection of underground objects by GPR [2] (see Fig. 5). One part of PML terminates the dispersive earth media, and the other terminates the

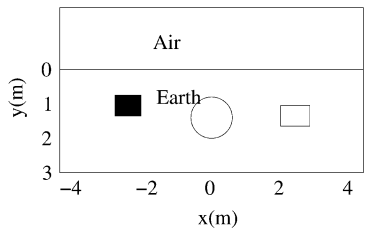

Fig. 5. Geometry of three objects buried in a dispersive earth, with a circle of radius 0.6 with centered at (0.0, 1.5). The rectangular on the left is $[-2.775, -2.025] \times [0.75, 1.35]$, and the one on the right is $[2.025, 2.775] \times [1.05, 1.65]$.

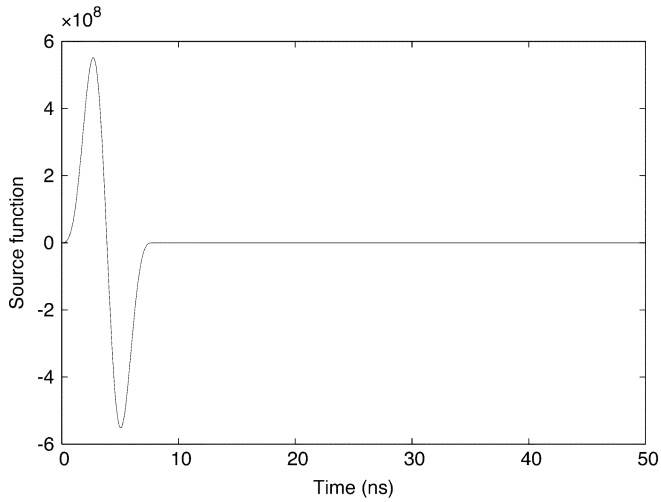

Fig. 6. First derivative of the Blackman–Harris window function used as the line source.

air. Fig. 5 shows a two-dimensional (2-D) GPR for the detection of objects buried in a dispersive earth medium. The rectangular object on the left is dispersive Debye medium (same parameters as before), while the other two anomalies are air voids.

The line current source used is the first derivative of the Blackman–Harris window function pointing in the z direction with a center frequency 200 MHz. The Blackman–Harris window function is given by

$$f(t) = \begin{cases} \sum_{n=0}^{3} a_n \cos(2n\pi t/T), & \text{if } 0 < t < T \\ 0, & \text{otherwise} \end{cases} \tag{41}$$

where T is the duration of the source function. The coefficients used are

$$a_0 = 0.353\,222\,22 \quad a_1 = -0.488$$
$$a_2 = 0.145 \quad a_3 = -0.010\,222\,222.$$

The source duration T is given by $T = 1.55/f_c$, where f_c is the center frequency of the source. For $f_c = 200$ MHz, the first derivative of the Blackman–Harris window function is shown in Fig. 6.

The initial computational domain is $[-4.05\text{ m}, 4.05\text{ m}] \times [-3\text{ m}, 3.75\text{ m}]$, terminated by a UPML of thickness $d = 0.75$ m. The discretization is $\Delta x = \Delta y = 0.075$ m and $\Delta t = 10$ ps. The local basis functions are the polynomials of degree 4, and the Runge–Kutta of order 4 is used for time discretization. The outer boundary of PML is assumed to be

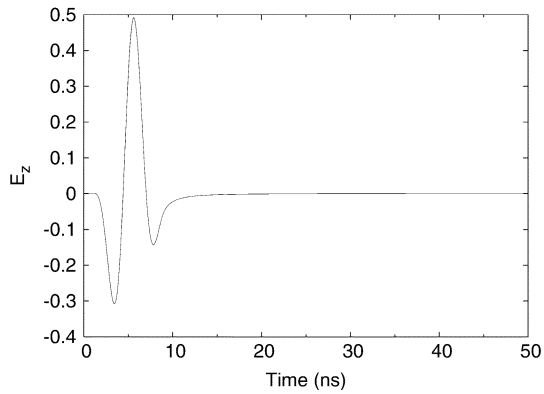

Fig. 7. Incident normalized field E_z at the receiver $(0.0375, -0.0375)$ when the source locates at $(0.4125, -0.0375)$.

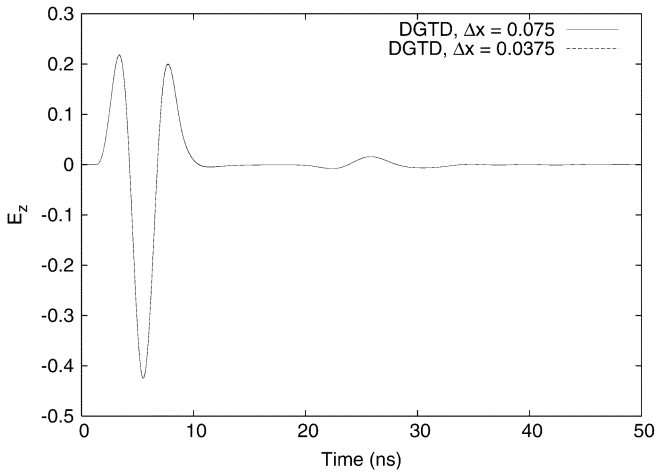

Fig. 8. Scattering E_z computed by using. The source and the receiver are located at $(0.0375, -0.0375)$ and $(0.4125, -0.0375)$, respectively. The L^2-norms of the error between them are 1.711×10^{-3}.

a PEC wall. It should be noted that η of the PML terminating different media is different [27]. In our computation, we set $\eta = 1/2$ in all the PMLs. We use the time step 10 ps to compute the incident wave.

The source is located at $(x, y) = (x_i, -0.0375)$ m, and the receivers are located at $(x_i + 0.375)$ m, where $x_i = -3.7125 + i \times 0.075, i = 0, 1, \ldots, 99$. To compute the scattering wave of the buried objects, we first compute the total wave when both the three objects and the ground are present. Then, we compute the incident wave when the ground is present, but the three objects are absent. The scattering wave is then obtained by subtracting the incident wave (see Fig. 7) from the total wave.

Mesh convergence: Before we compute the scattering wave at all receivers, we conduct the numerical convergence of DGTD with different meshes. For this purpose, we fix the source and the receiver at $(0.0375, -0.0375)$ and $(0.4125, -0.0375)$, respectively. Then, the scattering wave is computed with DGTD on $\Delta x = 0.075$ and $\Delta x = 0.0375$, and the L^2-norm of the difference between the two calculated scattering wave is 1.711×10^{-3} (see Fig. 8), thus confirming the mesh convergence. For the rest of the computations, we will use $\Delta x = 0.075$.

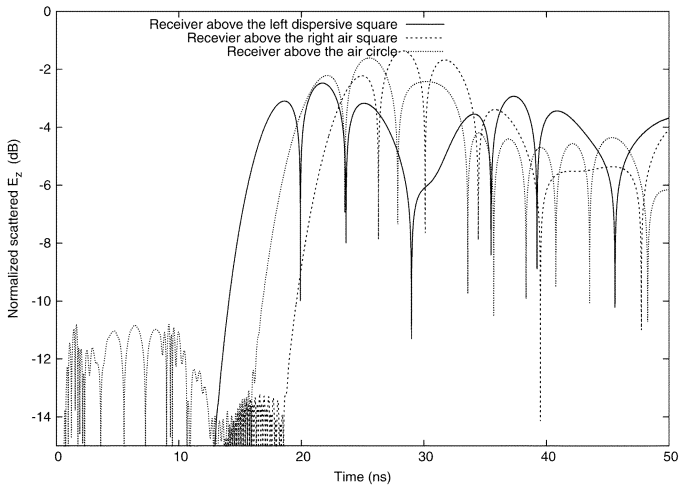

Fig. 9. Scattering E_z plotted with $2 \log_{10} |E_z|$.

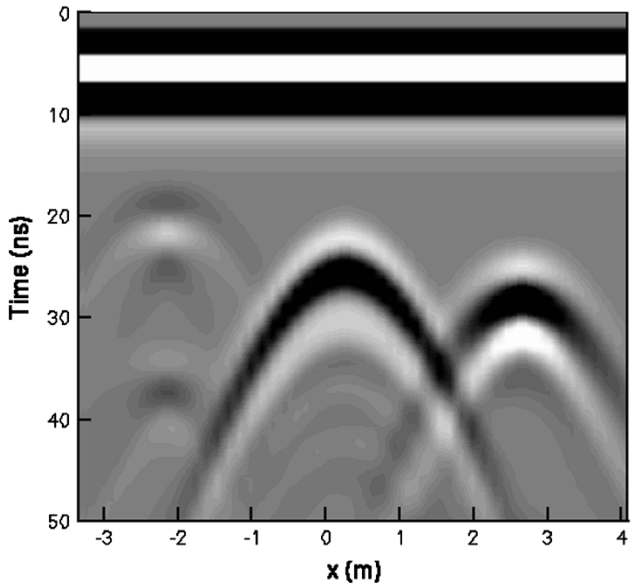

Fig. 10. Scattered field E_z at the different receivers and sources. The sources are at $(x_i, -0.0375)$ and the receivers at $(x_i + 0.375, -0.0375)$, where $x_i = -3.7125 + i \times 0.075, i = 0, 1, 2, 3, \ldots, 99$.

Fig. 9 shows the scattering wave E_z at three locations above the buried objects. Fig. 10 is the contour of the scattering waves at all receivers. The horizontal axis indicates the locations of the receivers, while the vertical axis is the time. The effect of the dispersion of the left most rectangle is seen clearly in the pattern of its scattering wave.

IV. Conclusion

We have developed a discontinuous Galerkin time-domain algorithm for general dispersive media, and the linear Debye media and the UPML terminating the computational domain are handled in a unified manner with the auxiliary differential equations method. The DGTD provides high-order accuracy in treating arbitrary shape of scatters and the temporal convolution of the electric field.

REFERENCES

[1] K. S. Yee, "Numerical solution of initial boundary value problems involving Maxwell's equations in isotropic media," *IEEE Trans. Antennas Propag.*, vol. AP-14, no. 3, pp. 302–307, May 1966.

[2] Q. H. Liu and G.-X. Fan, "Simulations of GPR in dispersive media using a frequency-dependent PSTD algorithm," *IEEE Trans. Geosci. Remote Sens.*, vol. 37, no. 5, pp. 2317–2324, Sep. 1999.

[3] G.-X. Fan and Q. H. Liu, "Multidomain pseudospectral time-domain simulations of scattering by objects buried in lossy media," *IEEE Trans. Geosci. Remote Sensing*, vol. 40, no. 6, pp. 1366–1273, Jun. 2002.

[4] W. Cai and S. Z. Deng, "An upwinding embedded boundary method for Maxwell's equations in media with material interfaces: 2-D case," *J. Comput. Phys.*, vol. 190, pp. 1–31, 2003.

[5] A. Ditkowski, K. Dridi, and J. S. Hesthaven, "Convergent cartesian grid methods for Maxwell's equations in complex geometries," *J. Comput. Phys.*, vol. 170, no. 1, pp. 39–80, Jun. 2001.

[6] B. Cockburn, S. Hou, and C.-W. Shu, "TVB Runge–Kutta local projection discontinuous Galerkin finite element method for conservation laws IV: The multidimensional case," *Math. Comput.*, vol. 54, pp. 545–581, 1990.

[7] B. Cockburn and C.-W. Shu, "Runge–Kutta discontinuous Galerkin methods for convection-dominated problems," *J. Sci. Comput.*, vol. 16, pp. 173–261, 2001.

[8] T. Warburton, "Application of the discontinuous Galerkin method to Maxwell's equations using unstructured polymorphic hp-finite elements," in *Proc. Int. Symp. Discontinuous Galerkin Methods*, 1999.

[9] J. S. Hesthaven and T. Warburton, "High-order/spectral methods on unstructured grids I. Time-domain solution of Maxwell's equations," NASA Langley Research Center, Hampton, VA, NASA/CR-20010210836 ICASE Rep. 2001-6, Mar. 2001.

[10] D. A. Kopriva, S. L. Woodruff, and M. Y. Hussaini, "Computation of electromagnetic scattering with a nonconforming discontinuous spectral element method," *Int. J. Numer. Meth. Eng.*, vol. 53, pp. 105–122, 2002.

[11] T. Lu, P. Zhang, and W. Cai, "Discontinuous Galerkin methods for dispersive and lossy Maxwell's equations and PML boundary conditions," *J. Comput. Phys.*, vol. 200, pp. 549–580, 2004.

[12] R. J. Luebbers, F. P. Hunsberger, K. Kunz, R. Standler, and M. Schneider, "A frequency-dependent finite-difference time-domain formulation for dispersive materials," *IEEE Trans. Electromagn. Compat.*, vol. 32, no. 3, pp. 222–227, Aug. 1990.

[13] R. J. Luebbers, D. Steich, and K. Kunz, "FDTD calculation of scattering from frequency-dependent materials," *IEEE Trans. Antennas Propag.*, vol. 41, no. 9, pp. 1249–1257, Sep. 1993.

[14] F. Kelley and R. J. Luebbers, "Piecewise linear recursive convolution for dispersive media using FDTD," *IEEE Trans. Antennas Propag.*, vol. 44, no. 6, pp. 792–797, Jun. 1996.

[15] T. Kashiwa and I. Fukai, "A treatment by FDTD method of dispersive characteristics associated with electronic polarization," *Microw. Opt. Tech. Lett.*, vol. 3, pp. 203–205, 1990.

[16] R. M. Joseph, S. C. Hagness, and A. Taflove, "Direct time integration of Maxwell's equations in linear dispersive media with absorption for scattering and propagation of femtosecond electromagnetic pulse," *Opt. Lett.*, vol. 16, no. 18, pp. 1412–1414, Sep. 1991.

[17] J. L. Young, "Propagation in linear dispersive media: Finite difference time-domain methodologies," *IEEE Trans. Antennas Propag.*, vol. 43, no. 4, pp. 422–426, Apr. 1995.

[18] D. M. Sullivan, "Frequency-dependent FDTD methods using Z transforms," *IEEE Trans. Antennas Propag.*, vol. 40, no. 10, pp. 1223–1230, Oct. 1992.

[19] J. P. Berenger, "A perfectly matched layer for the absorption of electromagnetic waves," *J. Comput. Phys.*, vol. 114, no. 2, pp. 185–200, Oct. 1994.

[20] Z. S. Sacks, D. M. Kingsland, R. Lee, and J.-F. Lee, "A perfectly matched anisotropic absorber for use as an absorbing boundary condition," *IEEE Trans. Antennas Propag.*, vol. 43, no. 12, pp. 1460–1463, Dec. 1995.

[21] R. W. Ziolkowski, "Time-derivative Lorentz model-based absorbing boundary condition," *IEEE Trans. Antennas Propag.*, vol. 45, no. 10, pp. 1530–1535, Oct. 1997.

[22] M. Dubiner, "Spectral methods on triangles and other domains," *J. Sci. Comp.*, vol. 6, pp. 345–390, Dec. 1991.

[23] S. Z. Deng and W. Cai, "Numerical modeling of optical coupling by whispering gallery modes between microcylinders," *J. Opt. Soc. Amer., A*, 2005, to be published.

[24] J. C. Butcher, *The Numerical Analysis of Ordinary Differential Equations: Runge–Kutta and General Linear Methods*. New York: Wiley, 1987.

[25] S. Gottlieb and L.-A. J. Gottlieb, "Strong stability preserving properties of Runge–Kutta time-discretization methods for linear constant coefficient operations," *J. Sci. Comput.*, vol. 18, no. 1, pp. 83–109, Feb. 2003.

[26] M.-H. Chen, B. Cockburn, and F. Reitich, "High order RKDG methods for computational electromagnetics," *J. Sci. Comput.*, to be published.

[27] A. Taflove and S. C. Hagness, *Computational Electromagnetics: The Finite-Difference Time-Domain Method*, 2nd ed. Boston, MA: Artech House, 2000.

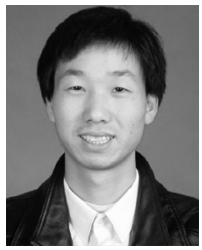

Tiao Lu received the B.S. and Ph.D. degrees in computational mathematics from Peking University, Beijing, China, in 1999 and 2004, respectively

He is currently with the Laboratory of Mathematics and Mechanization and the School of Mathematical Science, Peking University. His research interests include computational electromagnetics and the analysis of the wave propagation in inhomogeneous media.

Wei Cai received the Ph.D. degree in applied mathematics from Brown University, Providence, RI, in 1989.

He joined the Department of Mathematics, University of North Carolina (UNCC), Charlotte, in 1989 as an Assistant Professor and later became an Associate Professor in 1995. During the 1995–1996 period, he joined the Department of Mathematics, University of California, Santa Barbara, as an Assistant Professor and then became an Associate Professor. Since 1999, he has been a Full Professor in the Department of Mathematics, UNCC. His research interest includes computational electromagnetics for parameter extraction for computer packaging and VLSI designs and photonic waveguides.

Pingwen Zhang received the Ph.D. degree in computational mathematics from Peking University, Beijing, China, in 1992.

He is currently with the Laboratory of Mathematics and Mechanization and the School of Mathematical Sciences, Peking University. From 1992 to 1994, he was an Assistant Professor in the School of Mathematical Science, Peking University and became an Associate Professor in 1994. Since 1996, he has been a Professor. He is the Director of the School of Mathematical Science and the Executive Deputy Director of the Center for Computational Science and Engineering, Peking University. He is also the Vice Chairman of the China Society for Computational Mathematics. His research interests include multiscale modeling, analysis and computational methods, and computational mathematics and its application. He is an Executive Editor of the *Journal of Computational Mathematics* (in Chinese) and the *Journal of Computational Physics* (in Chinese). He is also an Associate Editor of *Communications in Mathematical Sciences*.

Dr. Zhang received the Medalist of Wu'si Youth Award, National Science Fund for Distinguished Young Scholars, and Changjiang Professor in 2002.